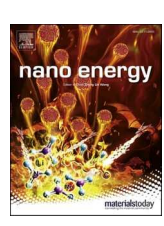
ELSEVIER

Contents lists available at ScienceDirect

Nano Energy

journal homepage: www.elsevier.com/locate/nanoen





Wireless, flexible, self-powered sensor to analyze head impact kinematics

Gerardo L. Morales-Torres^a, Ian González-Afanador^a, Bianca M. Dávila-Montero^b, Juan Pastrana^a, Henry Dsouza^a, Nelson Sepúlveda^{a,*}

- ^a Department of Electrical and Computer Engineering, Michigan State University, East Lansing 48824, MI, United States
- ^b Department of Mechanical Engineering, Michigan State University, East Lansing 48824, MI, United States

ARTICLE INFO

Keywords: Head impact kinematics Self-powered sensors Wearable sensors Wireless human monitoring Brain injury

ABSTRACT

This work presents a prototype of a wireless, flexible, self-powered sensor used to analyze head impact kinematics relevant to concussions, which are frequent in high-contact sports. Two untethered, paper-thin, and flexible sensing devices with piezoelectric-like behavior are placed around the neck of a human head substitute and used to monitor stress/strain in this region during an impact. The mechanical energy exerted by an impact force –varied in locations and magnitudes— is converted to pulses of electric energy which are transmitted wirelessly to a smart device for storage and analysis. The wireless prototype system is presented using a microcontroller with an integrated Bluetooth Low Energy module. The static and dynamic characteristics of the transmitted signal are then compared to signals from accelerometers embedded in a head substitute, to map the sensor's output to the angular velocity and acceleration during impacts. It is demonstrated that using only two sensors is enough to detect impacts coming from any direction; and that placing multiple external sensors around the neck region could provide accurate information on the dynamics of the head, during a collision, which other sensors fail to capture.

1. Introduction

A global estimate of 69 million people suffer from a traumatic brain injury (TBI) each year, with North America having the highest incidence [1]. In the United States, 223,135 people were hospitalized due to TBI in 2019, while 64,362 died from TBI-related deaths in 2020, as reported by the Centers of Diseases Control and Prevention (CDC) [2]. A concussion, also known as a mild traumatic brain injury (mTBI), is defined by the CDC as a bump, blow, or jolt to the head, or hit to the body that causes the head and brain to move quickly back and forth [3]. These can have a wide range of symptoms like headaches, nausea, fatigue, and problems with speech. More severe and lasting symptoms can include loss of consciousness, disabilities, coma, depression, and memory problems [4]. After a concussion, the brain remains in a vulnerable state for about a week. Suffering another concussive event during this period can lead to even greater damage and a higher likelihood of developing long-lasting effects [5]. Around 3.8 million sports-related concussions happen each year, and many of these injuries go unreported and undiagnosed [6]. Even multiple undiagnosed micro-concussions, provoked by milder impacts below the concussion range, can lead to significant symptoms [7,8]. Therefore, it is vital to detect when a person receives a mTBI,

especially in high-impact sports like American football (where 300,000 concussions are estimated to happen each year [9]), so they can be removed from harm's way and avoid more severe injury.

The Wayne State Tolerance Curve (WSTC) [10], Gadd Severity Index (GSI) [11], and Head Injury Criteria (HIC) [12] are metrics used to determine the severity of an impact using the linear acceleration of the head. However, angular acceleration has been determined to play a larger role in most mTBIs [13], since it generates strains within the brain, leading to increased tissue damage [14]. Current concussion-monitoring technology mounted in commercially available American football helmets is commonly referred to as the Head Impact Telemetry (HIT) System, which measures linear and angular accelerations [15]. The main drawback of this technology resides in the sliding effect between the helmet and the athlete's head. Since the sensors are located inside the helmet, it is uncertain whether they experience the same kinematics of the head during collision [16,17]. A solution to this was attempted by the X-Patch, wireless skin-affixed accelerometers attached behind the ear and in a mouth guard [18]. However, the peak accelerations captured by this system presented high inaccuracy [19], so there is still a need to overcome these issues.

In the quest for new sensors that address the aforementioned

E-mail address: sepulve6@msu.edu (N. Sepúlveda).

 $^{^{\}ast}$ Corresponding author.

problems, this work builds upon the attachment of Ferro-Electret Nano-Generator (FENG) sensors directly on the neck [20]. The FENG is a flexible, thin polypropylene (PP) film treated to induce the formation of electric dipoles which yields piezoelectric properties. It can harvest mechanical energy when its dipoles are deformed by an external force, generating charge accumulation, which results in an electrical output [21]. This makes them an attractive choice for self-powered sensing and energy-harvesting applications [22–24]. Their raw electrical output can also be processed and analyzed to extract additional information. In previous work, it was shown that, when placed directly on the neck, the first derivative of the FENG's output voltage during a whiplash can be mapped to the angular velocity of the head [20]. In other words, the device converts the mechanical energy of the neck's movement during an impact into an electrical signal that is correlated to the angular velocity of the head, allowing the monitoring of head impact kinematics.

A similar device to the one reported here is an ultra-stretchable wearable strain sensor with a conductive layer that changes the electrical resistance when it is stretched or bent [25]. It is also adhesive to human skin, making it a wearable strain sensor for human motion. However, this system has not been used to analyze impacts on the head, and its sensing element is not self-powered as the FENG. Thus, the resistive-based device would need additional electric components to fully convert the sensed signal, which will unavoidably add volume to the overall system and hinder its practicality in wearable applications especially for cases with constant and abrupt large deflections. The development of self-powered sensors is an essential component towards wearability.

In this work, a wireless portable prototype system is presented. It combines the FENG device with a simple signal conditioning circuit and a small-form-factor microcontroller with an integrated Bluetooth Low Energy (BLE) module. This advances the technology so that in the future it can be easily worn and used by athletes and TBI patients as a wearable sensor. This work also increases the sensing capabilities by using two FENG devices simultaneously, placed on the neck of a human head substitute. To determine how effective this arrangement is at capturing impacts from multiple directions, impact tests with different simulated head orientations were performed. The output signals from the FENGs during these tests are recorded wirelessly, analyzed, and compared to

angular velocity recorded by accelerometers inside the head to validate the system's performance at mapping impacts.

2. Methods

The setup for this project has three main elements: (i) the FENG patches which convert mechanical energy from impact to an electrical signal, (ii) the mechanical setup used to generate the impact on the head, (iii) and the electrical circuit used to capture, condition, and send the signal from each FENG.

2.1. Patch design

The locations of each FENG on the neck are shown in Fig. 1a, where one is on the back and the other on the left side (i.e., the patches are 90° from each other). Hereinafter, they will be referred to as "back FENG" and "side FENG" for simplicity. The FENG's design is the same as in previous work [20], with the addition of components to make a wearable prototype that enables data transfer wirelessly, which will be presented in another section. The fabrication procedure for these devices has been discussed at length in previous work [26]. Briefly explained, as shown in Fig. 1b, the FENGs (dimensions: 5 cm x 1 cm, thickness: ~100 μ m each) consist of deposited metal electrodes on both sides of a PP thin film containing micro "quasi-dipoles", encapsulated in Kapton tape with electrical leads coming out (not shown). Applying mechanical stress to the film reshapes its dipoles, which generates charge accumulation resulting in an electric potential difference between the electrodes [27]. This phenomenon is referred to as "quasi-piezoelectricity" and provides an electrical output due to the flow of charge across a load connected between those electrodes (electrical leads). A thin layer of polydimethylsiloxane (PDMS) is glued with epoxy to one side of the FENG. Two layers of therapeutic kinesiology tape (K-Tape) covered each side of the device, creating the patch. The patches were then fixed to the neck with hose clamps on both ends of the K-tape. This design allowed the K-tape to apply pressure to the FENG when the neck stretches, generating the FENG's electrical output.

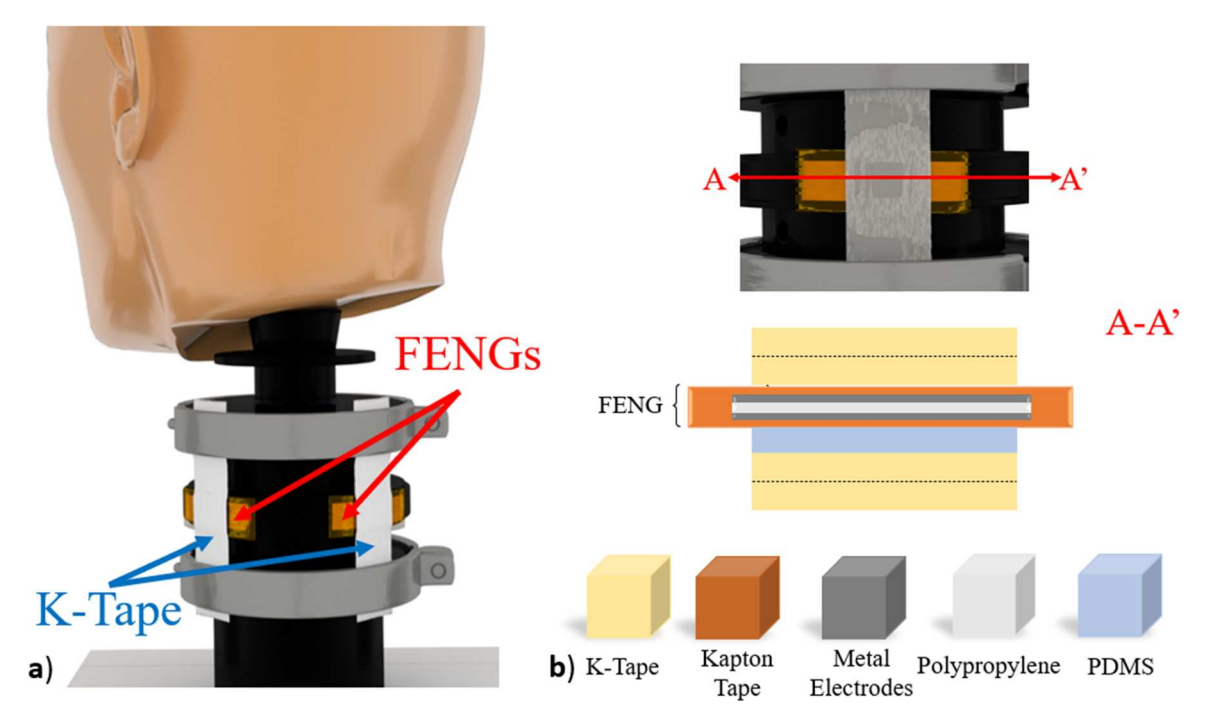


Fig. 1. a) FENG patches' locations on the neck: back and left side (i.e., 90° apart). b) FENG patch cross-section.

2.2. Head and impactor setup

The drop tower setup for impact testing is presented in Fig. 2a. A Hybrid III head and neck form assembly (hereinafter referred to as the dummy) from Humanetics (Hybrid III 50th Male, Standard ATD 78051–218-H), often used in crash test experiments [15,28], was

attached to a stationary beam to serve as the test subject. Inside the dummy head, there is a triaxial accelerometer with integrated triaxial angular rate (DTS-6DX PRO) which is used to capture angular velocities during impact experiments in this work. The orange cylinder-like device in Fig. 2a is the impactor, which is attached to a movable beam dropped in "free-fall" (i.e., using only gravity) to hit the head. It was 3D printed

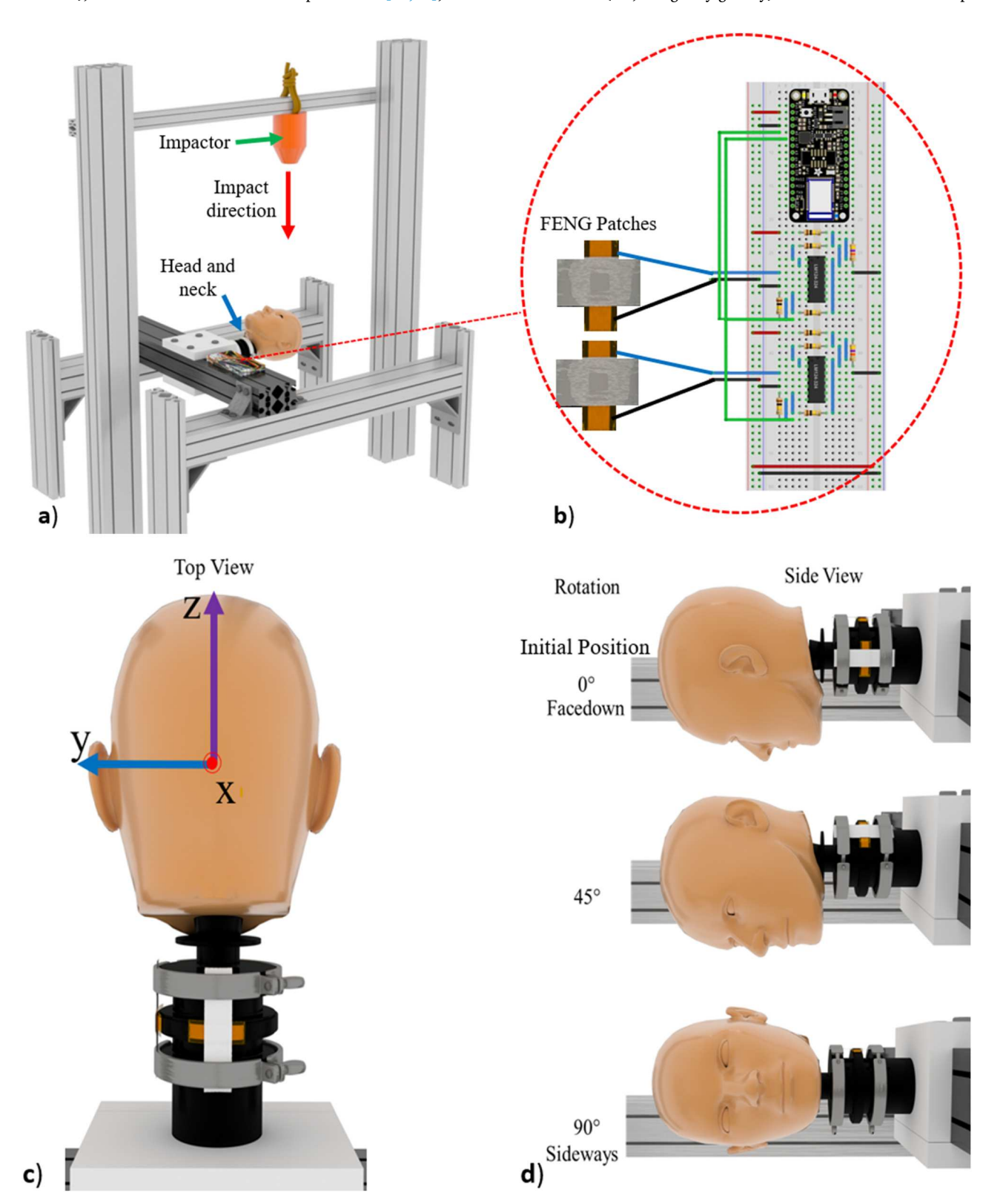


Fig. 2. a) The mechanical setup used to generate impacts. b) Electrical setup used to capture FENGs' output. c) Dummy head axes from top view while head faces down. d) The three different positions used for the experiments in this work (rotation along the z-axis).

out of polylactic acid (PLA) and designed to distribute the load evenly upon impact. It should be noted, that while the FENG patches are on the neck, the microcontroller and electrical system that captures the FENGs' output, shown in Fig. 2b and which will be covered in the next section, are not attached to the dummy. The orientation of the dummy head axes is shown in Fig. 2c. As shown in Fig. 2d, three head positions were of interest for impact analysis: face down (initial position), head rotated 45° , and head rotated 90° along the z-axis with respect to the initial position. For simplicity, the positions will be referred to as facedown, 45° , and sideways.

In this work, the impact force was varied by changing the load of the impactor: 1.5 kg, 2.5 kg, and 3.5 kg. Table 1 shows the theoretical speed, momentum, and kinetic energy for each load. The calculated values were obtained from the 45° configuration. The height from the head to the tip of the impactor before being released was 0.66 m. This number varied slightly for the facedown and sideways positions, where this distance changed by a maximum of ± 0.02 m, due to the elliptical shape of the head around the z-axis. Margins of errors have been included to consider variations from the other configurations. Friction was neglected, and the values were obtained using simple physics equations shown in Section 2 of the supplementary material.

2.3. Electrical design

The FENG patches were connected to a microcontroller (Adafruit Feather nRF52 Bluefruit LE from Adafruit Industries), shown in Fig. 2b. This will be referred to as the "MC" from here on out. The MC (dimensions: $5.1 \times 2.3 \times 8$ cm, mass: 5.7 g), powered by a 3.7 V, 400 mAh Lithium Polymer (LiPoly) battery, can capture analog data, convert it to digital, and send it wirelessly via Bluetooth to smart devices in an estimated outdoors range of 73-103 m [29,30]. It can only acquire input voltages in the 0-3.3 V range, while the FENGs can produce voltages above and below this span. Thus, connecting the FENGs' output directly to the MC will result in loss of data and possible damage to the MC. To address this, two quadruple operational amplifiers (LM324N) were implemented in the design, powered by a programmable external triple output DC power supply set to 5 V, 1 mA. Fig. 3 shows the electrical signal condition circuit used for each FENG, represented as a voltage pulse source. The FENG is connected to a voltage follower configuration (1st operational amplifier stage), where loading effects are isolated from the FENG device. Then, using an inverting summing amplifier (2nd operational amplifier stage), a voltage bias of 3.3 V (coming from the MC) was added to the FENG's output voltage. This stage also attenuates the voltage signal by a factor of 0.47 before feeding the output to a simple inverting amplifier with unity gain (3rd operational amplifier stage) to obtain a positive output voltage V_{out} that the MC can safely read.

2.4. Data acquisition process

Once the MC receives the processed signal from the FENG devices, it is sent to the BluefruitConnect App on a tablet (iPad 7th generation). This app was developed by Adafruit Industries to interact with their devices, and it was used in this work to receive and store the data sent wirelessly by the MC via Bluetooth protocol using universal asynchronous receiver-transmitter (UART) communication. This type of communication is usually performed between two wired devices,

Table 1
Theoretical conditions at the moment of impact.

Parameter	Calculated Values		
Mass (kg)	1.5	2.5	3.5
Speed (m/s)	3.6 ± 0.05	3.6 ± 0.05	3.6 ± 0.05
Momentum (kg·m/s)	$\textbf{5.4} \pm \textbf{0.07}$	9 ± 0.12	12.6 ± 0.17
Kinetic Energy (J)	9.72 ± 0.3	16.2 ± 0.45	22.68 ± 0.7

transmitting and receiving serial data bit by bit [31]. Bluetooth UART emulates the same behavior of a wired UART system allowing the exchange of 20 bytes of data at a time [32]. The data is then forwarded to a computer for further analysis.

During testing, the impactor is released and allowed to free fall towards the head. Once it is detected to be at 0.39 m away from the head, both the MC and SLICEWARE, the software from DTS which collects the data from its accelerometers inside the head (6DX-PRO), start data acquisition simultaneously, capturing two seconds worth of data following the flow depicted in Fig. 4. The impactor detection was done with the help of an ultrasonic sensor along with an Arduino UNO microcontroller (not shown) that generates a trigger to initiate data recording. It should be noted that the sampling frequencies between the MC and SLICEWARE software are not equal. The MC, which has a RAM of 64 KB [30], was storing three variables (time, and two FENG sensors' outputs) without external memory. A sampling rate of 1 kHz for two seconds made the MC run smoothly without compromising the memory. On the other hand, SLICEWARE had a sampling frequency of 5 kHz. This was the lowest sampling rate, using the program's default settings, at which it could capture the accelerometers' output without exhibiting aliasing. The raw data of the FENGs was interpolated to reach the same number of samples as the angular velocity recorded, thus allowing for synchronizing signals with time and enabling a correlation (i.e., mapping) process that would become crucial for calibration and validation purposes. A fourth-order Butterworth low-pass filter was used to filter the angular velocities at a cutoff frequency of 100 Hz, as previously done by Dsouza et al. [20]. However, by capturing the FENGs' output with the MC, it was prone to pick up more ambient noise, so a tighter cutoff frequency of 20 Hz was used to get a clearer signal using the same type of filter. The derivatives of the FENGs' voltages were calculated using MATLAB and compared to the angular velocities measured by the accelerometers.

3. Results and discussion

Facedown and sideways impacts to the head were evaluated first. Fig. 5a shows the orientation of the head axes during facedown impacts, and Fig. 5b shows the first derivative of the back FENG's output voltage and the angular velocity around the y-axis. Similarly, Fig. 5c and d show the orientation and outputs during a sideways impact (rotation around the x-axis, side FENG's output derivative). The impactor mass was 2.5 kg for both tests presented here. For validation purposes, data was captured from both FENG sensors (located at the back and side of the neck) during each experiment. During the facedown test, the most active sensor is the back FENG, since the impact vector was perpendicular to that FENG's position, producing hyperflexion directly proportional to the impact. However, as the movement generated by the facedown impact does not generate any lateral stress on the neck, the side FENG does not perceive the impact, and its output stays close to zero. For the sideways test, the most active FENG sensor is the side FENG (since it is perpendicular to the impact vector in this case) and the back FENG on the neck did not produce any significant signal. Therefore, Fig. 4b and d only shows the most active FENGs' outputs, but the ones not presented here can be found in the videos of the supplementary material.

During the experiments, the derivative of the FENG's output behaves similarly to the angular velocity only during the first peak, when both sensors (i.e., the accelerometers and the FENG sensors) experienced the same force dynamics, as shown in Fig. 5b and d. This can be explained by considering the sensing mechanism for the accelerometers and the mechanical dynamics of the experiment. During the test, the mechanical setup does not allow for the head to oscillate after the impact. The mechanical input from the impactor is not a pure pulse signal, since the impactor is dropped in free fall and keeps exerting a downward force after the impact, due to its weight. Thus, when the impactor is dropped, it generates a heavily damped, short-lived oscillation response before settling, which is reflected after the first peak in the output signal from

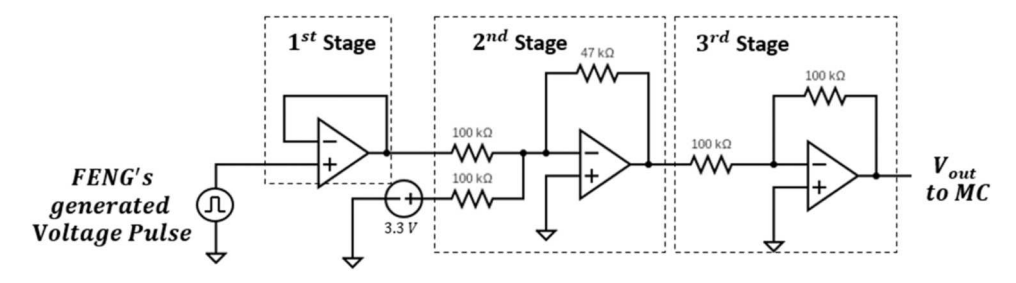


Fig. 3. Schematic of the electrical circuit used to condition the FENG's output voltage before being sent to the microcontroller.

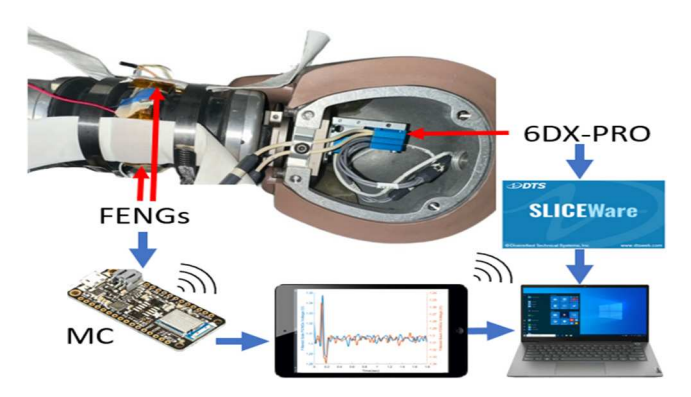


Fig. 4. Data acquisition process. FENGs' output gets captured by MC and is sent wirelessly to a tablet and then a computer. Accelerometers' output gets captured by SLICEWARE Software on the computer.

the accelerometers inside the dummy head. Also, although both sensors are actively being monitored simultaneously for the same impact experiments, the FENG sensors are located at the neck region of the dummy head, picking up stress-strain signals away from the location of impact. However, the most crucial piece of information for an impact is captured in the peak [33], for which both signals (angular velocity and FENG) show very similar dynamic responses and allow for their comparison and correlation. Thus, during the first peak –which records the maximum effect of the impact– the derivative of the FENG's output can be mapped to the angular velocity [20].

As shown in Fig. 5b and d, the amplitude of the angular velocity (measured by the accelerometers) is higher during the facedown impact than in the sideways impact. The reason for this is that this model of the dummy head's mechanics is not designed to be equally compliant in every spatial direction, since it is originally designed for frontal automotive crash tests [34]. The human head substitute can receive impacts from the sides, but its design mostly considers rotational movement along the y-axis. This is also reflected in the small delay exhibited by the

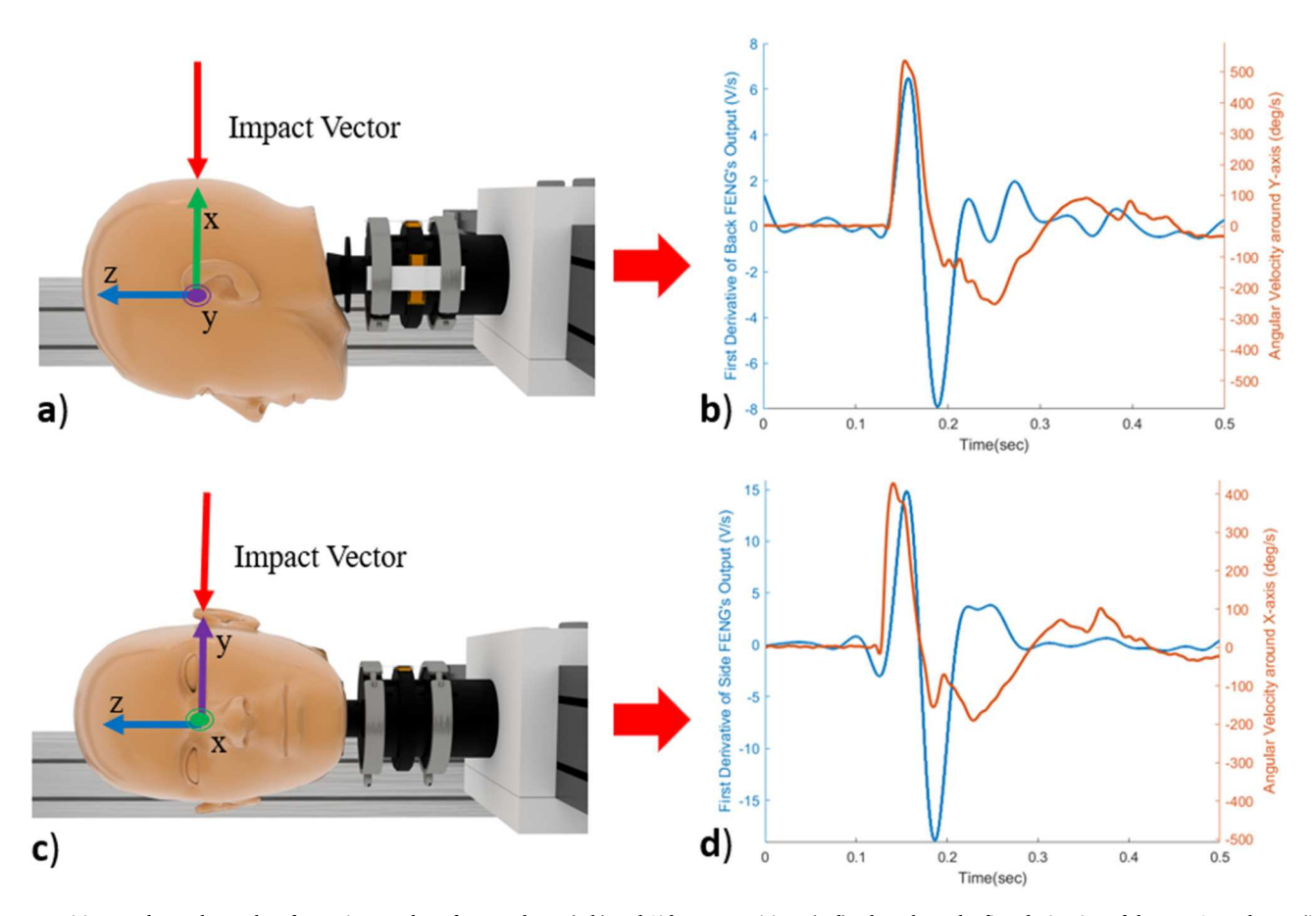


Fig. 5. Positions and sample results of experiments done for Facedown (a-b) and Sideways Positions (c-d). Plots show the first derivative of the FENGs' voltages (i.e., FENGs signals) and angular velocities (i.e., accelerometer signal) for a 2.5 kg impactor.

side FENG's output (when compared to the back FENG's), where tests were performed to examine this delay and it was determined that it is also attributed to the design of the neck. However, even though the mechanics of a sideways movement (i.e., rotation along the x-axis) of the dummy head is different from facedown movement (i.e., rotation along the y-axis), both FENGs located orthogonal to the movement in each case were able to capture the kinematics of the neck generated by the impacts. Contrary to the angular velocity behavior, the peak voltage derivative of the FENG is greater while the head rotates along the x-axis (sideways impact) than along the y-axis (facedown impact). However, this can also be due to the neck's design, meaning that it is stiffer around the x-axis rotation, leading to a higher rate of change in the FENG's output voltage.

Fig. 6 shows the measurements of the FENGs' voltage derivatives and the corresponding angular velocities during a 45° impact. Both the derivative of the voltage of the back FENG and the angular velocity along the y-axis, shown in Fig. 6b, have the same behavior shown in Fig. 5b when the head is hit facedown. This is also true for the side FENG and the angular velocity along the x-axis in Fig. 6c when compared to Fig. 5d, with a significant delay in the rate of change of the FENG's output due to the neck's design. Interestingly, the angular velocity is greater along the x-axis than on the y-axis. The head was expected to have more rotation along the y-axis than the x-axis, as shown in Figs. 5b and 5d, but due to the head's anatomy, the impact received at the 45° configuration was not perpendicular to the center of gravity of the head,

explaining the greater rotation along the x-axis. Fig. 6d shows the magnitudes of the FENGs and the angular velocities of both axes, where the peak of interest of the FENG is not the absolute maximum, but the peak that is reflected during the absolute maximum of the velocity. As previously mentioned, these peaks are the ones that record the maximum effect of the impact. During those peaks, the first derivative of the FENG and the angular velocity present similar behavior.

Fig. 7 (left column) shows the confidence intervals of the peaks of interest from the FENGs' responses and their corresponding angular velocities peaks. This analysis was done by capturing multiple impacts with the impactor at different loads (1.5, 2.5, 3.5 kg presented in Table 1) for each head position, and then analyzing the resultant FENG $\frac{dV}{dt}$ and the corresponding angular velocity magnitude for each configuration, as it was done in Fig. 6d. The peaks of focus of $\frac{d^2V}{dt^2}$ and angular acceleration are also shown in Fig. 6 (right column) for each head position. The peak magnitudes of the FENGs' output and the velocities for the 45° experiment are smaller than when the impact is perpendicular to the head's rotation axis. This is also true for the peaks of the second derivative of the FENGs and angular acceleration. However, even though the peaks of the magnitudes vary between head positions while maintaining the same impact force, the FENGs' measured output still shows a strong linear correlation with the angular velocity.

The peak derivatives of the FENGs showed a positive correlation (R > 80 %) with the angular velocities. Furthermore, the second derivatives of the FENGs also showed a good correlation (R > 75 %) with the

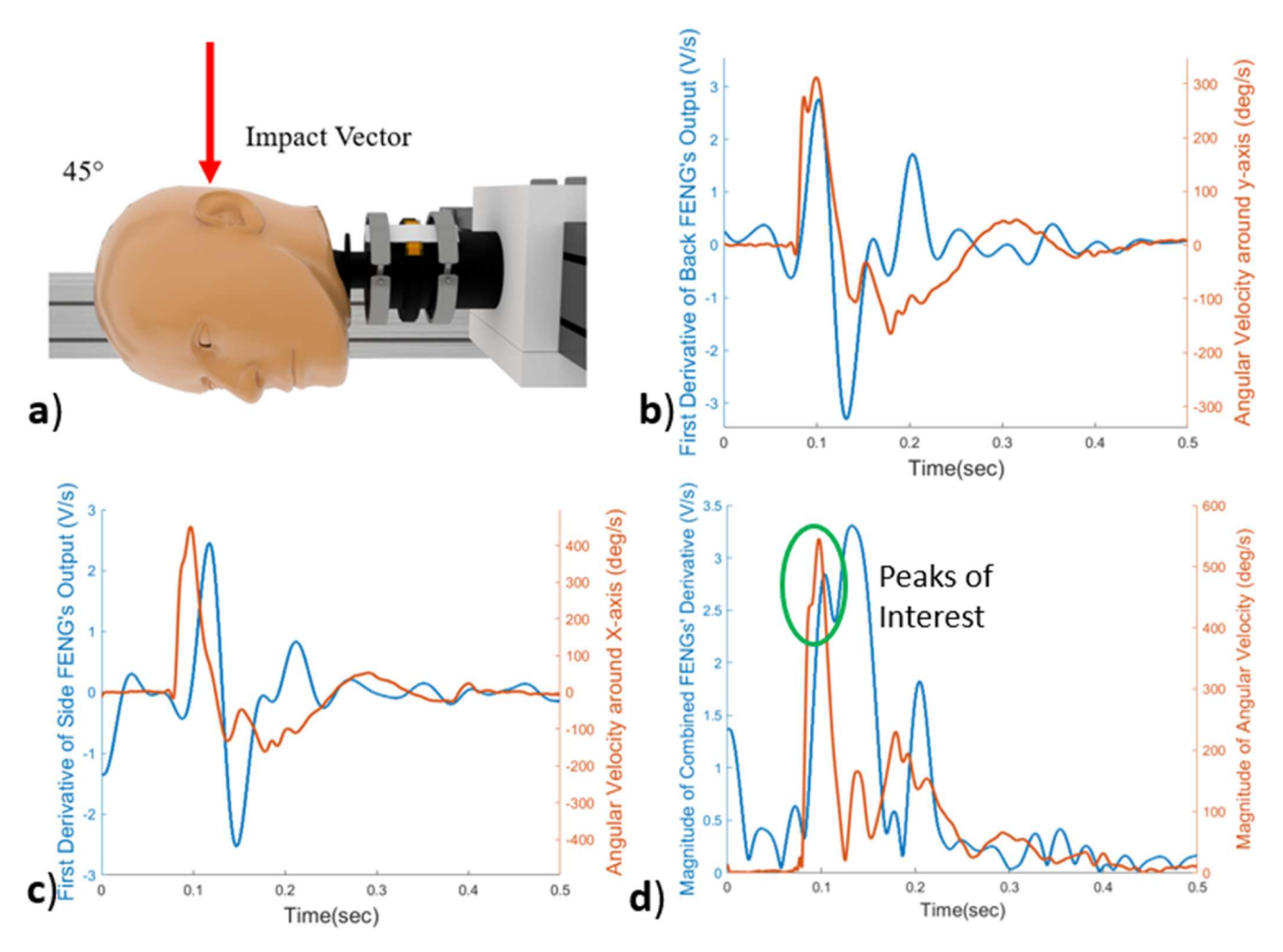


Fig. 6. a) 45° head position, b) Derivative of the voltage of back FENG and respective angular velocity, c) Derivative of the voltage of side FENG and respective angular velocity, and d) Magnitudes of the derivatives (from FENG) and angular velocity (from accelerometers). The results shown are for the 2.5 kg impactor experiment.

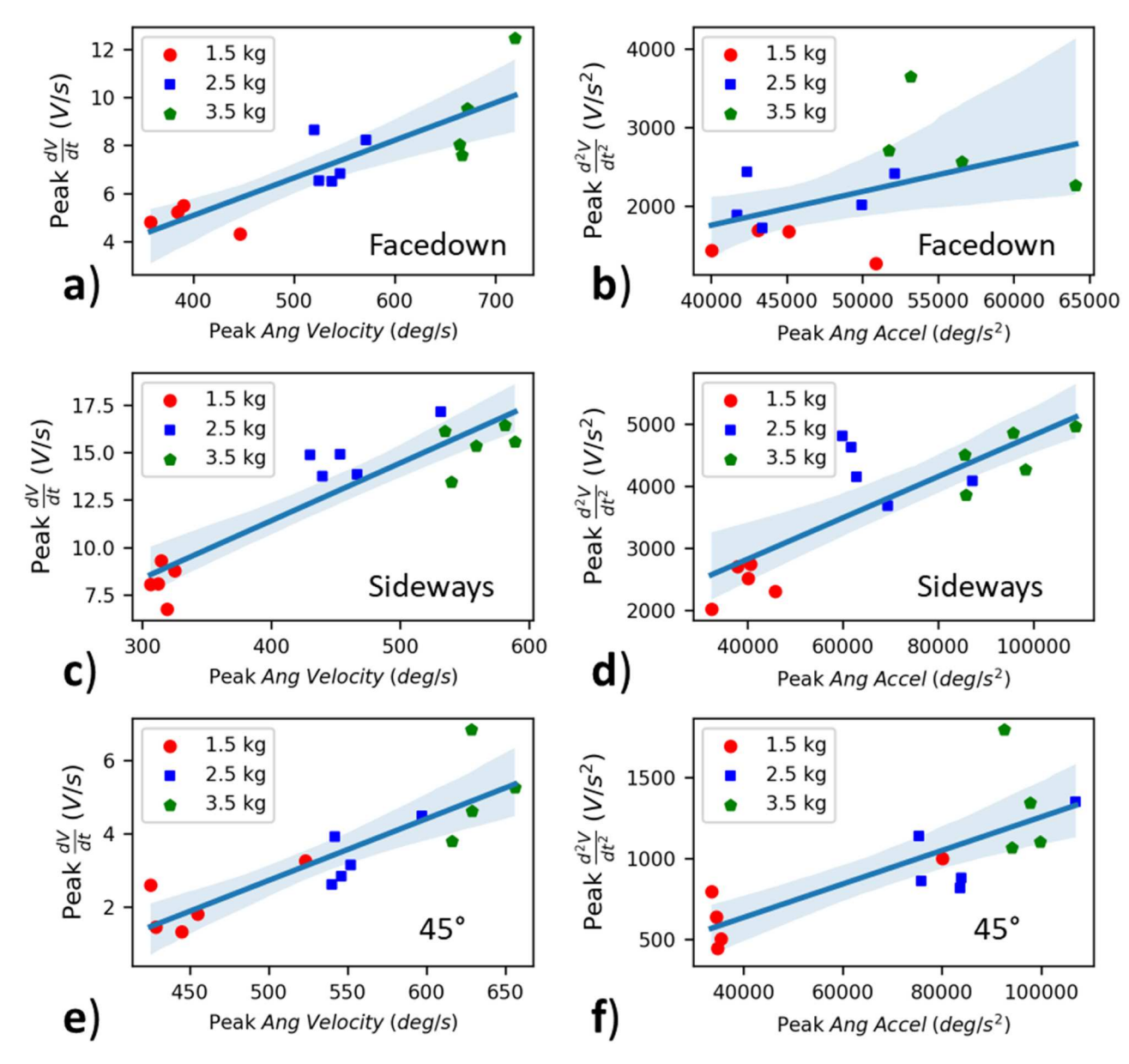


Fig. 7. a, c, e) Peak voltage derivatives of the FENGs vs. Peak Angular Velocities for the different dummy head positions. b, d, and f) Peak of the second derivatives of the FENGs vs. Peak Angular Accelerations for the different dummy head positions.

angular acceleration, except for the facedown configuration, seen in Fig. 7b. An explanation for this is that while on facedown, the back FENG is already bent due to the head's weight. The same happens with the other head positions, but while on sideways and 45° , as previously discussed, the neck is stiffer rotating around the x-axis. This means that while on facedown, the back FENG is significantly bent before impact, making the rate of change of the first derivative behave differently compared to the other dummy positions, presenting peaks with little correlation with the angular acceleration (R = 47 %).

4. Conclusion

This work builds on the approach of using FENG devices to analyze head impact kinematics. It demonstrated how multiple devices can capture the head dynamics in different impact orientations and showed that the output can be easily wirelessly transmitted. The setup used for these tests makes the neck to be bent before impact and does not allow the head to have sustained oscillations after the hit, since the impactor stays on top of the head after the main impact, adding a constant

downward force due to its weight, thus preventing the head and neck from moving freely. This means that this mechanical setup does not allow measuring impacts coming from opposite sides of the FENGs' placement, because it does not allow the part of the neck that contains the FENGs to stretch enough and apply pressure to it. However, it was proved by Dsouza et. al [20] that the FENG is capable of capturing impacts from the opposite side of the FENG's location if the head can oscillate freely. In conjunction with previous work, these experiments support the claim that by only using two FENGs on the neck, an impact can be detected from any direction, though its magnitude might not be fully captured without additional FENG devices. Covering half the neck with FENG patches might present more accurate readings for impacts to the head with different angles and force magnitudes, also allowing better readings of normal and faster head rotations.

CRediT authorship contribution statement

G.M.-T.: Conceptualization, Methodology, Software, Investigation, Formal analysis, Data Curation, Writing-Original Draft **I.G.-A.:**

Visualization, Methodology, Software, Writing - Review & Editing B.D.-M.: Conceptualization, Resources, Investigation J.P.: Conceptualization, Visualization, Writing - Review & Editing H.D.: Conceptualization, Validation, N.S.: Supervision, Project administration, Funding acquisition, Writing - Review & Editing.

Declaration of Competing Interest

The authors declare that they have no known competing financial interests or personal relationships that could have appeared to influence the work reported in this paper.

Data Availability

Data will be made available on request.

Acknowledgments

This work was supported by the National GEM Consortium. This material is also based upon work supported by the National Science Foundation under Grant No. ECCS-1854750. Finally, the authors would like to thank Prof. Ricardo Mejia-Alvarez for access to some of the equipment used in the experiments.

Appendix A. Supporting information

Supplementary data associated with this article can be found in the online version at doi:10.1016/j.nanoen.2023.108835.

References

- M.C. Dewan, et al., Estimating the global incidence of traumatic brain injury, J. Neurosurg. (2018) 1–18, https://doi.org/10.3171/2017.10.JNS17352.
- [2] "TBI Data | Concussion | Traumatic Brain Injury | CDC Injury Center," Mar. 21, 2022. (https://www.cdc.gov/traumaticbraininjury/data/index.html) (accessed Apr. 10, 2023).
- [3] "Mild TBI and Concussion | Concussion | Traumatic Brain Injury | CDC Injury Center," Nov. 14, 2022. (https://www.cdc.gov/traumaticbraininjury/concussion/index.html) (accessed Apr. 10, 2023).
- [4] "Traumatic brain injury Symptoms and causes," Mayo Clinic. (https://www.ma yoclinic.org/diseases-conditions/traumatic-brain-injury/symptoms-causes/syc-2 0378557) (accessed Apr. 10, 2023).
- [5] R. Vagnozzi, et al., Temporal window of metabolic brain vulnerability to concussions: mitochondrial-related impairment—part I, Neurosurgery 61 (2) (2007) 379–389, https://doi.org/10.1227/01.NEU.0000280002.41696.D8.
- [6] "Concussion in Athletes | Michigan Medicine." (https://www.uofmhealth.org/conditions-treatments/brain-neurological-conditions/concussion-athletes-neurosport #:~:text=The%20Center%20for%20Disease%20Control%20estimates%20that% 205-10%25,can%20lead%20to%20prolonged%20symptoms%20and%20long-term%20consequences) (accessed Apr. 10, 2023).
- [7] "Micro concussions may alter football players' brains," Apr. 09, 2018. (https://www.medicalnewstoday.com/articles/321430) (accessed Apr. 10, 2023).
- [8] "Micro Concussions Happen Often in Sports," YourCareEverywhere. (https://yourcareeverywhere.com/health-research/health-insights/brain-and-nerve-care-insights/micro-concussions-happen-often-in-sports.html) (accessed Apr. 10, 2023).
- "Concussion Statistics and Facts | UPMC | Pittsburgh," UPMC Sports Medicine. (htt ps://www.upmc.com/services/sports-medicine/services/concussion/about/facts -statistics) (accessed Apr. 10, 2023).
- [10] E.S. Gurdjian, W.A. Lange, L.M. Patrick, M.E. Thomas, Impact injury and crash protection, Plast. Reconstr. Surg. 46 (5) (1970) 505, https://doi.org/10.1097/ 00006534-197011000-00018.
- [11] C.W. Gadd, Use of a Weighted-Impulse Criterion for Estimating Injury Hazard (1966), 660793, https://doi.org/10.4271/660793.
- [12] R. Eppinger, S. Kuppa, R. Saul, E. Sun, Supplement: development of improved injury criteria for the assessment of advanced automotive restraint systems: II, Mar.

- 2000. Accessed: Apr. 10, 2023. [Online]. Available: \(\lambda \text{https://rosap.ntl.bts.go}\) v/view/dot/14739\).
- [13] S. Kleiven, Why most traumatic brain injuries are not caused by linear acceleration but skull fractures are, Front. Bioeng. Biotechnol. 1 (2013), https://doi.org/ 10.3389/fbioe.2013.00015 (Available), (https://www.frontiersin.org/articles/).
- [14] "Biomechanical Basis of Traumatic Brain Injury," Clinical Gate, Mar. 26, 2015. \(\https://clinicalgate.com/biomechanical-basis-of-traumatic-brain-injury/\) (accessed Apr. 10, 2023).
- [15] J.G. Beckwith, R.M. Greenwald, J.J. Chu, Measuring head kinematics in football: correlation between the head impact telemetry system and hybrid III headform, Ann. Biomed. Eng. 40 (1) (2012) 237–248, https://doi.org/10.1007/s10439-011-0422-2
- [16] R. Jadischke, D.C. Viano, N. Dau, A.I. King, J. McCarthy, On the accuracy of the Head Impact Telemetry (HIT) System used in football helmets, J. Biomech. 46 (13) (2013) 2310–2315, https://doi.org/10.1016/j.jbiomech.2013.05.030.
- [17] "Understanding concussions: Testing head-impact sensors," University of Michigan News, Jan. 29, 2014. (https://news.umich.edu/understanding-concussions-testin g-head-impact-sensors/) (accessed Apr. 10, 2023).
- [18] "X2 Biosystems Unveils Next Generation Wearable Head Impact Monitor," PRWeb. (https://www.prweb.com/releases/2016/02/prweb13237354.htm) (accessed Apr. 10, 2023)
- [19] D.B. Camarillo, P.B. Shull, J. Mattson, R. Shultz, D. Garza, An instrumented mouthguard for measuring linear and angular head impact kinematics in American football, Ann. Biomed. Eng. vol. 41 (9) (. 2013) 1939–1949, https://doi.org/ 10.1007/s10439-013-0801-v.
- [20] H. Dsouza, J. Pastrana, J. Figueroa, I. Gonzalez-Afanador, B.M. Davila-Montero, N. Sepúlveda, Flexible, self-powered sensors for estimating human head kinematics relevant to concussions, Sci. Rep. 12 (1) (2022) 8567, https://doi.org/10.1038/ s41598-022-12266-6.
- [21] W. Li, D. Torres, T. Wang, C. Wang, N. Sepúlveda, Flexible and biocompatible polypropylene ferroelectret nanogenerator (FENG): on the path toward wearable devices powered by human motion, Nano Energy 30 (2016) 649–657, https://doi. org/10.1016/j.nanoen.2016.10.007.
- [22] Y. Cao, et al., Flexible ferroelectret polymer for self-powering devices and energy storage systems, ACS Appl. Mater. Interfaces 11 (19) (2019) 17400–17409, https://doi.org/10.1021/acsami.9b02233.
- [23] Q. Zhong, J. Zhong, B. Hu, Q. Hu, J. Zhou, Z.L. Wang, A paper-based nanogenerator as a power source and active sensor, Energy Environ. Sci. 6 (6) (2013) 1779, https://doi.org/10.1039/c3ee40592c.
- [24] Y. Zhang, et al., Ferroelectret materials and devices for energy harvesting applications, Nano Energy 57 (2019) 118–140, https://doi.org/10.1016/j nanoen.2018.12.040.
- [25] Q. Zhang, X. Liu, L. Duan, G. Gao, Ultra-stretchable wearable strain sensors based on skin-inspired adhesive, tough and conductive hydrogels, Chem. Eng. J. 365 (2019) 10–19, https://doi.org/10.1016/j.cej.2019.02.014.
- [26] W. Li, et al., Nanogenerator-based dual-functional and self-powered thin patch loudspeaker or microphone for flexible electronics, Nat. Commun. 8 (1) (2017) 15310, https://doi.org/10.1038/ncomms15310.
- [27] J. Pastrana, et al., Electrode effects on flexible and robust polypropylene ferroelectret devices for fully integrated energy harvesters, ACS Appl. Mater. Interfaces 12 (20) (2020) 22815–22824, https://doi.org/10.1021/ acsami.0c02019.
- [28] E.S. Walsh, P. Rousseau, T.B. Hoshizaki, The influence of impact location and angle on the dynamic impact response of a Hybrid III headform, Sports Eng. 13 (3) (2011) 135–143, https://doi.org/10.1007/s12283-011-0060-9.
- [29] "Understanding Bluetooth Range," Bluetooth® Technology Website. (https://www.bluetooth.com/learn-about-bluetooth/key-attributes/range/) (accessed Apr. 19, 2023).
- [30] "Nordic Semiconductor Infocenter." (https://infocenter.nordicsemi.com/index.jsp ?topic=%2Fstruct_nrf52%2Fstruct%2Fnrf52832.html) (accessed Apr. 19, 2023).
- [31] "UART: A Hardware Communication Protocol Understanding Universal Asynchronous Receiver/Transmitter | Analog Devices." (https://www.analog.com/en/analog-dialogue/articles/uart-a-hardware-communication-protocol. html#:~:text=By%20definition%2C%20UART%20is%20a%20hardware%20communication%20protocol,the%20transmitting%20device%20going%20to%20the%20receiving%20end) (accessed Apr. 10, 2023).
- [32] "Bluetooth UART Service," Microsoft MakeCode. (https://makecode.microbit.or g/reference/bluetooth/start-uart-service) (accessed Apr. 10, 2023).
- [33] A. Post, T. Blaine Hoshizaki, M.D. Gilchrist, M.D. Cusimano, Peak linear and rotational acceleration magnitude and duration effects on maximum principal strain in the corpus callosum for sport impacts, J. Biomech. 61 (2017) 183–192, https://doi.org/10.1016/j.jbiomech.2017.07.013.
- [34] "Frontal Impact ATDs." (https://www.humaneticsgroup.com/products/anthropomorphic-test-devices/frontal-impact) (accessed Apr. 10, 2023).